Changes in the Arctic Oscillation under increased atmospheric greenhouse gases

Aiming Wu[1], William W. Hsieh[1]

George J. Boer[2] and Francis W. Zwiers[2]

1 Dept. of Earth and Ocean Sciences, University of British Columbia
Vancouver, BC V6T 1Z4, Canada
Tel: (604) 822-3932, Fax: (604) 822-6088
E-mail: awu@eos.ubc.ca

2 Canadian Centre for Climate Modelling and Analysis
University of Victoria, Victoria, BC V8W 2Y2, Canada

1

Abstract

The Arctic Oscillation (AO) under increased atmospheric concentration of greenhouse gases (GHG) was studied by comparing an ensemble of simulations from 13 coupled general circulation models with GHG at the pre-industrial level and at the late 20th century level, for November to March. The change in the linear AO pattern as GHG increased reveals positive sea level pressure (SLP) anomalies centered over the Gulf of Alaska, and weaker negative SLP anomalies over eastern Canada and North Atlantic – a pattern resembling the nonlinear AO pattern arising from a quadratic relation to the AO index. This quadratic AO pattern itself has positive SLP anomalies receding from Europe but strengthening over the Gulf of Alaska and surrounding areas as GHG increased. This study points to the importance of the nonlinear structure in determining how the linear oscillatory pattern changes when there is a change in the mean climate.

1   Introduction

The Arctic Oscillation (AO) is the leading mode of atmospheric variability over the extratropical Northern Hemisphere [*Thompson and Wallace*, 1998, 2001]. Through principal component analysis (PCA), the spatial AO pattern is commonly obtained from the first empirical orthogonal function (EOF) of the mean sea level pressure (SLP) anomaly field, while the associated principal component (PC) time series serves as an AO index.

The AO index has gradually risen since the 1960s with historic highs in the early 1990s. It has been suggested that this positive trend in the AO index significantly contributed to the observed warming trend over Eurasia and North America, accounting for as much as 50% of the winter warming over Eurasia [*Thompson et al.*, 2000]. It is also notable that the AO index has been decreasing in recent years; with these recent data included, *Cohen and Barlow* [2005] found that the overall trends for the past 30 years were weak to nonexistent.

Most climate models under increasing greenhouse gases (GHG) forcing showed a positive trend in the AO index [*Gillett et al.*, 2002]. Comparing the observed SLP trends with those simulated in response to natural and anthropogenic influence in a suite of coupled general circulation models (CGCM), *Gillett et al.* [2005] found that while the simulated Southern Hemisphere SLP trends were consistent with observations, the simulated Northern Hemisphere SLP trends were far too weak. Some authors [*e.g., Scaife et al.*, 2005] suggested that a well-resolved stratosphere in the model could be important for simulating the AO trend.

Besides trends in the AO index, the AO spatial anomaly pattern may also respond to changes in natural and anthropogenic forcing. Analyzing the data from an ensemble of 201-year simulations by the Canadian Centre for Climate Modelling and Analysis (CCCma) coupled climate model forced by

3

changing GHG concentrations and aerosol loading [*Flato and Boer*, 2001], *Fyfe et al.* [1999] found that the model simulated an essentially unchanged AO spatial pattern superimposed on a forced climate pattern. AO also has nonlinear structure. For example, composite analyses reveal that during positive and negative AO phases, the associated atmospheric anomaly patterns are not simply anti-symmetric to each other [*Pozo-Vázquez et al.*, 2001; *Wu et al.*, 2006]. Using nonlinear projection via a neural network (NN) approach to study nonlinear atmospheric teleconnections, *Hsieh et al.* [2006] found that, in addition to the classic (i.e. linear) AO spatial pattern, there is significant variability that is associated quadratically with the AO index.

In this study, using data from 13 CGCMs, we found that despite the general similarity between the spatial AO pattern in the pre-industrial and in the current period, there are subtle changes which can be explained by nonlinear (mainly quadratic) AO behavior.

2   Data and methodology

2.1   Data

We studied simulations produced with 13 CGCMs for the Intergovernmental Panel on Climate Change (IPCC) Fourth Assessment Report, namely CCCma-CGCM3.1, CNRM-CM3, CSIRO-Mk3.0, GFDL-CM2.0, GISS-ER, IAP-FGOALS-g1.0, INM-CM3.0, IPSL-CM4, MIROC3.2, MIUB-ECHO-G, MRI-CGCM2.3.2, NCAR-CCSM3.0 and UKMO-HadCM3. See http://www-pcmdi.llnl.gov/ipcc/model_documentation/ipcc_documentation.php for details. We used two simulations from each model, one from the integration with the GHG concentrations fixed at the pre-industrial (PI) level, and the other from the committed climate change experiments (CMT) where the GHG and aerosols were fixed at the level of the late 20th century. The various model runs ranged

4

in length from 100 to 500 years.

The observed monthly SLP data from NCAR [*Trenberth and Paolino*, 1980] during January 1950 to December 2005 were also used, with SLP anomalies calculated by subtracting the monthly climatological means from 1950-2005. After weighting the anomalies by the square root of the cosine of the latitude, PCA was performed on the November to March monthly anomaly data over the N. Hemisphere from 20°N to 90°N, with the standardized first PC defined as the AO index. A longer record of monthly SLP data from 1850 to 2004, namely the Hadley Center SLP Version 2 (HadSLP2)[*Allan and Ansell*, 2006], was also used.

For the model SLP data from each CGCM, the climatological monthly mean from the PI run was subtracted to give the anomalies both for the PI run and for the CMT run. For each CGCM, PCA was performed on the November to March monthly SLP anomalies in the PI run, with the standardized first PC taken to be the AO index. To keep a consistent definition of the AO index between the PI and CMT experiments for each CGCM, the CMT anomalies were projected to the first EOF from the PI experiment, then standardized (using the mean and standard deviation from the PI experiment) to obtain the AO index. The mean of the AO index in each of the 13 model CMT runs are 0.13, 0.08, 0.05, 0.11, 0.07, -0.02, 0.10, 0.36, 0.03, 0.33, 0.07, 0.14 and -0.07, respectively. The average over the 13 values is 0.11, compared to 0.16, the change in the mean AO index over the period 1950-2004 relative to that over the period 1850-1900 (from the HadSLP2 data). We acknowledge that it is only a rough comparison, as forcing is constant in the CMT runs (although the climate is not in equilibrium), while forcing is not constant in the real world especially during the latter half of the 20th century.

2.2   Quadratic polynomial fit

In *Hsieh et al.* [2006], the nonlinear relation between the N. Hemisphere winter SLP anomalies and the AO index was found be basically quadratic. Hence we will fit a quadratic polynomial between the gridded SLP anomalies ($\mathbf{y}$) and the AO index (x) (with no time lag between x and $\mathbf{y}$),

$$\mathbf{y} = \mathbf{a}x + \mathbf{b}x^2 + \mathbf{c}, \tag{1}$$

where $\mathbf{a}$ gives the classic linear AO pattern, while $\mathbf{b}$ gives the quadratic response pattern.

For each CGCM, a quadratic polynomial least squares fit was performed separately for the PI and CMT runs, and the linear and quadratic patterns were then ensemble averaged over the 13 CGCMs. For the shorter observational record, bootstrap resampling [*Efron and Tibshirani* 1993] was performed 400 times, where each bootstrap sample was obtained by randomly selecting (with replacement) one winter's data N times from the original record of N years. The linear and quadratic patterns were then ensemble averaged over the 400 quadratic polynomial fits.

3   Results

Figs. 1a and b show the ensemble mean of the linear AO pattern for the PI and CMT model runs, respectively, while Fig. 1c shows the corresponding results from observations for the period 1950-2005. The SLP anomaly patterns are visually quite similar to each other in Figs. 1a, b and c, except that in the model results the AO SLP anomalies are too strong over N. Pacific compared to the observations, where the AO is weaker over N. Pacific than over N. Atlantic and Europe.

Figs. 1d, e and f show the ensemble averaged quadratic pattern for the PI, CMT and observational data, respectively. Being quadratically associated with the AO index, these anomalies are excited during both the positive and negative phase of the AO index. Positive SLP anomalies centered over

the Gulf of Alaska extended from the N. Pacific to N. America, then through Greenland to Europe, while negative anomalies occurred over the North Atlantic. The magnitudes of the anomalies in these quadratic patterns are much weaker than those in the linear patterns, nevertheless, there is considerable similarity among these three quadratic patterns. Although the quadratic anomalies from observations have larger magnitude than those from the models, this could merely be sampling variability as the observed record is quite short. A similar nonlinear pattern is obtained when using the HadSLP2 data (not shown).

The quadratic pattern is also seen changing under increased GHG (cf. Figs. 1d and 1e): The positive anomalies receded from Europe but strengthened over the Gulf of Alaska and surrounding areas, suggesting that under enhanced GHG, the nonlinear AO behavior tends to occur farther from the Euro-Atlantic region.

The change in the classic linear AO pattern under enhanced GHG (Fig. 2) is somewhat similar to the quadratic patterns in Figs. 1d, e and f, especially Fig. 1e, suggesting that the change in the classic AO pattern is related to the nonlinear property of AO itself, as will be investigated below.

4   Discussion

We now examine the quadratic fit (1) to see what happens when there is a shift in the mean of x under climate change. Let $x = \overline{x} + x'$, and $\mathbf{y} = \overline{\mathbf{y}} + \mathbf{y}'$, where the overbar denotes the mean and the prime denotes the deviation. The mean of (1) gives

$$\overline{\mathbf{y}} = \mathbf{a}\,\overline{x} + \mathbf{b}\,\overline{x^2} + \mathbf{c}, \tag{2}$$

hence

$$\mathbf{y}' = (\mathbf{a} + 2\,\overline{x}\,\mathbf{b})x' + \mathbf{b}x'^2 + \mathbf{c}', \tag{3}$$

7

129 where $\mathbf{c}' = -\mathbf{b}\,\overline{x'^2}$. This implies that if the mean $\overline{x}$ is nonzero, the linear AO pattern given by $\mathbf{a} + 2\,\overline{x}\,\mathbf{b}$

130 would have imbedded the quadratic pattern $\mathbf{b}$. In the PI runs, $\overline{x} = 0$, so the linear AO pattern is $\mathbf{a}$;

131 but in the CMT runs, if $\overline{x} = \Delta$, then the linear pattern becomes $\mathbf{a} + 2\mathbf{b}\Delta$. The difference between

132 the linear patterns in CMT and in PI is thus $2\mathbf{b}\Delta$, hence the resemblance to the quadratic pattern,

133 as was indeed found between Fig. 2 and Fig. 1d or e.

134 Our results also imply Δ to be positive, since if Δ were negative, Fig. 2 would have displayed

135 opposite signed anomalies from Fig. 1e. The AO index has indeed been found to gradually rise in

136 observations [*Wallace and Thompson*, 2002] and in climate models under increasing GHG forcing

137 [*Gillett et al.*, 2002, 2003]. The change in the linear pattern in Fig. 2 is manifested most strongly in

138 the Gulf of Alaska, where it reaches about 0.4 hPa, whereas the quadratic pattern reaches about 0.4

139 hPa in the same area in Fig. 1e. To account for the change in the linear pattern by $2\mathbf{b}\Delta$ requires

140 $\Delta \approx 0.5$. A similar estimate in the Atlantic yields $\Delta \approx 0.3$, hence an average Δ of about 0.4 is needed.

141 However, in the CMT runs, Δ averaged only 0.11, a little less than 30% of the needed value.

142 There are two possibilities for the discrepancy: (a) The weak Δ results from the fact that the

143 CGCMs simulate SLP trends that are too weak in the N. Hemisphere [*Gillett et al.* 2005], and (b) our

144 assumption that Eq. (1) is unchanged as GHG increased is not strictly correct. For instance, in the

145 least squares fit, $\mathbf{a}$ is solved for in terms of variances and covariances involving $\mathbf{y}'$, x' and x'^2, which

146 have been assumed to be unchanged from PI to CMT.

5   Summary and conclusions

148 Data from multiple CGCM simulations with GHG concentrations at the PI level and at the late

149 20th century level (CMT) were used to reveal how AO changes under global warming. By fitting

a quadratic polynomial between the SLP anomalies and the AO index, we obtained the oscillatory patterns in the SLP that are linearly and quadratically related to the AO index. The linear pattern is the classic AO pattern, while the quadratic pattern shows positive SLP anomalies centered over the Gulf of Alaska stretching from northeast Pacific-N. America through Greenland to Europe, and weaker negative SLP anomalies over North Atlantic, in general agreement with the quadratic pattern extracted from observed data.

The change of the linear AO pattern under increased GHG (from PI to CMT) showed a SLP anomaly pattern which resembled the quadratic pattern. A small change in the mean of the AO index under increased GHG would modify the linear AO pattern due to the presence of the quadratic pattern. That the underlying nonlinear structure can alter the classic linear oscillations under changes in the mean background state is a new concept which may also apply to the other oscillations in our climate system.

The quadratic pattern of AO also exhibits changes from increased GHG, with the positive SLP anomalies receding from Europe while strengthening over the Gulf of Alaska and surrounding areas.

Acknowledgements

171   the CGCM data from the internet.

References

Allan, R. J., and T. J. Ansell (2006), A new globally complete monthly historical gridded mean sea level pressure data set (HadSLP2): 1850-2004. *J. Climate, 19*, 5816-5842.

Cohen, J., and M. Barlow (2005), The NAO, the AO, and global warming: How closely related? *J. Climate, 18*, 4498-4513.

Efron, B., and R. J. Tibshirani (1993), *An Introduction to the Bootstrap*, CRC, Boca Raton.

Flato G. M., and G. J. Boer (2001), Warming asymmetry in climate change simulations, *Geophys. Res. Lett., 28*, 195-198.

Fyfe, J. C., and G. J. Boer, and G. M. Flato (1999), The Arctic and Antarctic oscillations and their projected changes under global warming, *Geophys. Res. Lett., 26*, 1601-1604.

Gillett, N. P. et al. (2002), How linear is the Arctic Oscillation response to greenhouse gases? *J. Geophys. Res., 103* DOI:10.1029/2001JD000589.

Gillett, N. P., F. W. Zwiers, A. J. Weaver, and P. A. Stott (2003), Detection of human influence on sea level pressure, *Nature, 422*, 292-294.

Gillett, N. P., R. J. Allan, and T. J. Ansell (2005), Detection of external influence on sea level pressure with a multi-model ensemble, *Geophys. Res. Lett., 32*, L19714, DOI:10.1029/2005GL023640. 292-294.

Hsieh, W. W., A. Wu, and A. Shabbar (2006), Nonlinear atmospheric teleconnections, *Geophys. Res. Lett., 33*, L07714, doi:10.1029/2005GL025471

Pozo-Vázquez, D., M. J. Esteban-Parra, F. S. Rodrigo, and Y. Castro-Diez (2001), A study of NAO variability and its possible nonlinear influences on European surface temperature, *Clim. Dynam., 17*, 701-715.

Scaife, A. A., J.R. Knoght, G.K. Vallis, and C.K. Folland (2005), A stratospheric influence on the winter NAO and North Atlantic surface climate. *Geophys. Res. Lett., 32*, L18715, doi:10.1029/2005G-L023226.

Thompson, D. W. J., and J. M. Wallace (1998), The Arctic Oscillation signature in the wintertime geopotential height and temperature fields, *Geophys. Res. Lett., 25*, 1297-1300.

Thompson, D. W. J., J. M. Wallace, and G. C. Hegerl (2000), Annular modes in the extratropical circulation. Part II: Trends, *J. Climate, 13*, 1018-1036.

Thompson, D. W. J., and J. M. Wallace (2001), Regional climate impacts of the Northern Hemisphere annular mode, *Science, 293*, 85-89.

Trenberth, K.E., and D. A. Paolino (1980), The Northern Hemisphere sea level pressure data set: Trends, errors and discontinuities, *Mon. Wea. Rev., 108*, 855-872.

Wallace, J.M., and D. W. J. Thompson (2002), Annular modes and climate prediction. *Physics Today, 55*, 28-33.

Wu, A., W. W. Hsieh, A. Shabbar, G. J. Boer and F. W. Zwiers (2006), The nonlinear association between the Arctic Oscillation and North American winter climate, *Clim. Dynam.*, DOI: 10.1007/s00382-006-0118-8.

Figure captions

Figure 1: Ensemble averaged linear pattern (top row) and quadratic pattern (bottom row) of the SLP anomalies associated with the AO index. The left column shows the ensemble mean from 13 CGCM integrations forced with PI GHG concentrations, the middle column, from the same models but with the late 20th century (CMT) conditions, and the right column, the observed data (1950-2005). The shaded areas indicate statistical significance at the 5% level based on the t-test (in panels a, b, d and e), and based on the bootstrap distribution (in panels c and f). The contour interval is 1 hPa for the linear patterns, and 0.1 hPa for the quadratic patterns.

Figure 2: Changes in the linear AO pattern under increased GHG, i.e. Fig. 1b minus Fig. 1a. The contour interval is 0.05 hPa, with shaded areas significant at the 5% level from the t-test.
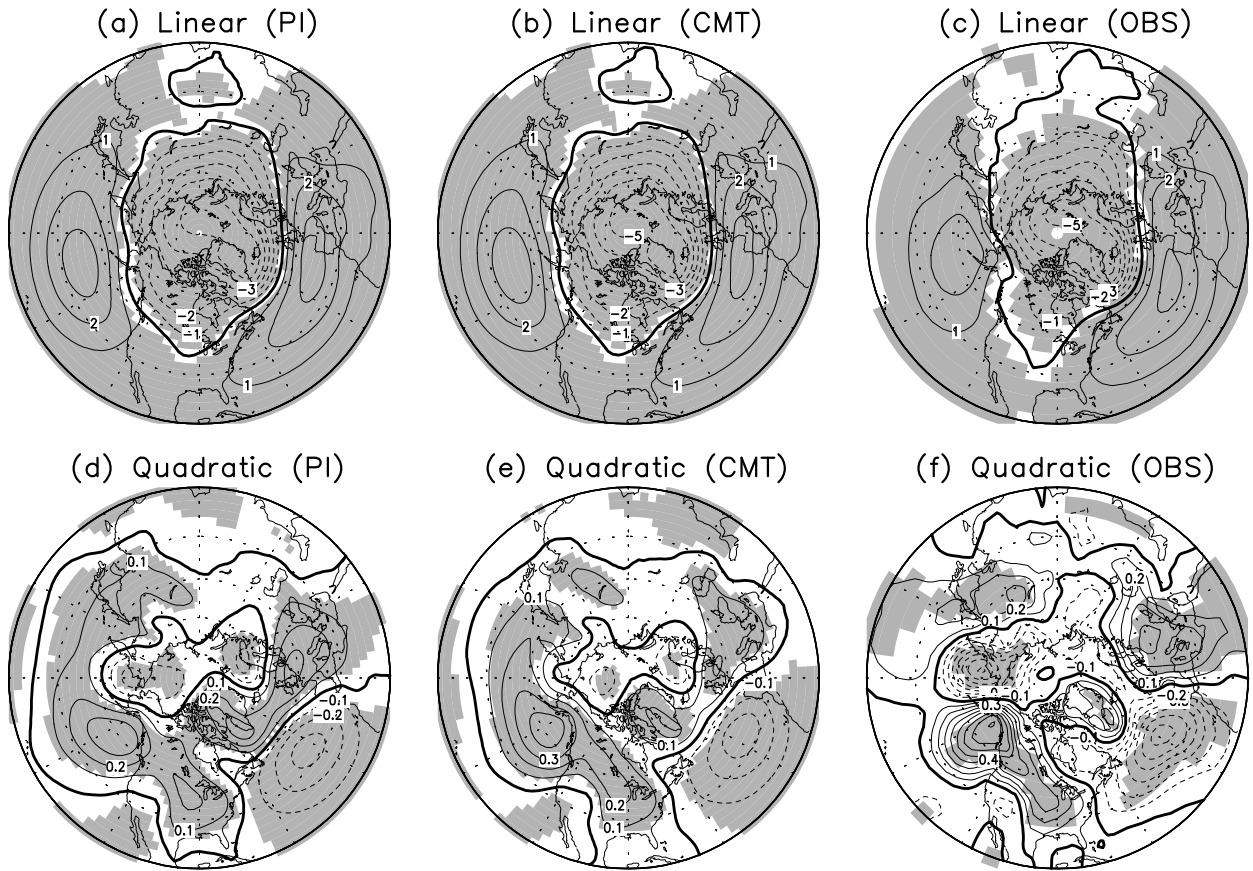
Figure 1: Ensemble averaged linear pattern (top row) and quadratic pattern (bottom row) of the SLP anomalies associated with the AO index. The left column shows the ensemble mean from 13 CGCM integrations forced with PI GHG concentrations, the middle column, from the same models but with the late 20th century (CMT) conditions, and the right column, the observed data (1950-2005). The shaded areas indicate statistical significance at the 5% level based on the t-test (in panels a, b, d and e), and based on the bootstrap distribution (in panels c and f). The contour interval is 1 hPa for the linear patterns, and 0.1 hPa for the quadratic patterns.
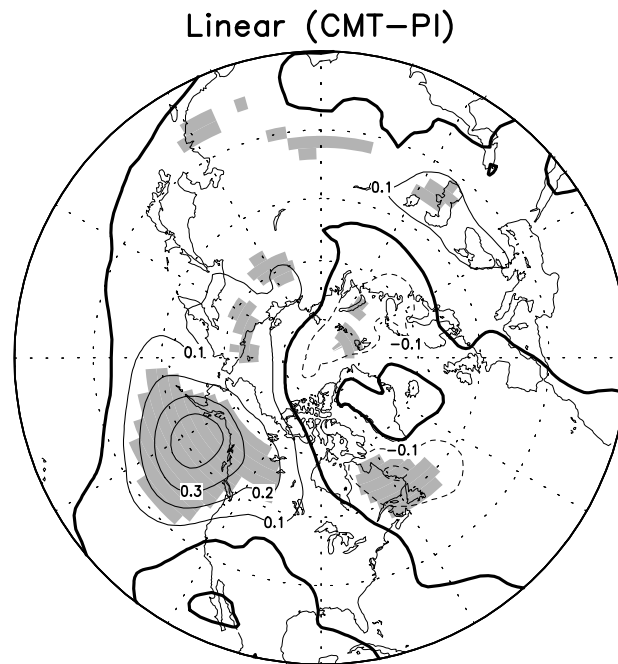
Figure 2: Changes in the linear AO pattern under increased GHG, i.e. Fig. 1b minus Fig. 1a. The contour interval is 0.1 hPa, with shaded areas significant at the 5% level from the t-test.